Surface Phase Diagram and Oxygen Coupling Kinetics on Flat and Stepped Pt Surfaces under Electrochemical Potentials

Ya-Hui Fang and Zhi-Pan Liu*

Shanghai Key Laboratory of Molecular Catalysis and Innovative Materials, Department of Chemistry, Center for Computational Science and Engineering, Fudan University, Shanghai 200433, China

Received: February 5, 2009; Revised Manuscript Received: April 14, 2009

Electrochemical reactions catalyzed by metal electrode, despite their huge importance in industry, are not well understood at the atomic level. In relevance to water electrolysis, the oxygen coupling reaction on Pt metal surfaces is systematically investigated in this work by combining periodic density functional theory calculations with a new theoretical approach to mimic the electrochemical environment. In our approach, the surface is explicitly polarized by adding/subtracting charges and the counter charges are placed as Gaussian-distributed plane charges in a vacuum. With this method, the surface phase diagrams for both the closed-packed Pt(111) and stepped Pt(211) are determined, which demonstrates that stepped surface sites can better accumulate oxidative species and thus reach to a higher local O coverage compared to Pt(111) at a given potential. The water environment is proved to affect the phase diagram marginally. By fully exploring the possible oxygen coupling channels on Pt surfaces, we show that the oxygen coupling reaction is kinetically difficult on metallic Pt surfaces below 1.4 V. There is no facile O coupling channels on Pt(111), as the barriers are no less than 1 eV. Although an O + OH → OOH reaction can eventually occur at the stepped sites with an increase of local O coverage and the calculated barrier is lower than 0.7 eV at 1.4 V (NHE), at such high potentials the (111) surface can already undergo surface oxidation due to the penetration of oxygen into sublayers. The theory thus indicates that oxygen evolution on Pt anode occurs on Pt surface oxides as dictated by thermodynamics and also demonstrates that the local surface structure and coverage can be more important in affecting the barrier of surface reactions than the electric fields.

1. Introduction

Recent years have seen tremendous progress in understanding solid/gas interface reactions at the atomic level.[1−4] On the other hand, electrocatalysis that occurs at the solid/liquid interface remains a highly challenging subject for both experimentalists and theoreticians.[5−7] Electrochemical reactions are not only catalyzed by solid electrode but also influenced by electrochemical potential and aqueous environment. Owing to the difficulty in applying most of the conventional surface science techniques in electrochemistry, the understanding of electrocatalytic reactions still falls far short of chemists' expectation. Aiming to shed light on the microscopic nature of electrocatalytic reactions, here we investigate the oxygen coupling reaction on Pt by first-principles theoretical methods, with particular emphasis on the surface structure, the electrochemical potential, the solvation effects on the surface phase, and activity.

The oxygen evolution reaction (OER: $H_2O \rightarrow {}^1/_2O_2 + 2H^+ + 2e$) as encountered in water electrolysis is one of the most important anodic reactions. Because the reaction causes the major energy loss in water electrolysis and is also involved in many applications concerning energy storage/conversion,[8,9] better anode materials for more efficient oxygen evolution have been consistently pursued for years.[10,11] It is known generally that the oxidative species (such as OH_{ad} and O_{ad}) dissociated from H_2O appear on the electrode at certain positive potentials, and by further increasing the potential, O_2 evolves originated from these surface oxidative species. In 1960s Bockris and co-workers suggested 14 possible routes for oxygen evolution on Pt according to experimental data.[12] They suggested that H_2O splitting may be the rate-determining step, while the oxygen coupling on the electrode may proceed via any combination of O and OH (e.g., O + O, O + OH, or OH + OH). The detailed mechanism for oxygen evolution at the atomic level is not established yet.

On the other hand, the recombination of oxygen atoms to form O_2 on Pt surfaces at ultrahigh vacuum (UHV) conditions was noticed to be extremely difficult, and it only occurs at very high temperatures from surface science experiments.[13] The reason why electrocatalysis can work at ambient conditions has been conventionally addressed by the empirical equation $\Delta G^{\ddagger} = \Delta G_0^{\ddagger}(U_0) - \beta F\eta$, which relates the change of barrier ($\Delta G^{\ddagger}$) to the variation of overpotential (η).[14] Here U_0 is the reversible potential (1.23 V for OER on Pt), F is Faraday's constant, and β is the transfer coefficient, usually taken as 0.5 (about 50% of work done by electric field is used to reduce the reaction barrier). The equation states that the activation barrier in electrocatalysis is linearly proportional to the applied overpotential. While β can only be determined by fitting experimental data, e.g., Tafel curves,[15] the microscopic nature of the barrier−potential relationship remains elusive.

In recent years, theoretical calculations have been used to probe the atomic level detail of electrochemical reactions, and some models to describe the electrochemical environment have been proposed. Anderson and co-workers developed a model applicable to several atom clusters by using the principle that the reaction center's electron affinity or ionization potential can be matched with the thermodynamic work function of the electrode.[16] They suggested that the channel of oxygen formation

* To whom correspondence should be addressed. E-mail: zpliu@fudan.edu.cn.

10.1021/jp901091a CCC: $40.75
Published on Web 05/08/2009

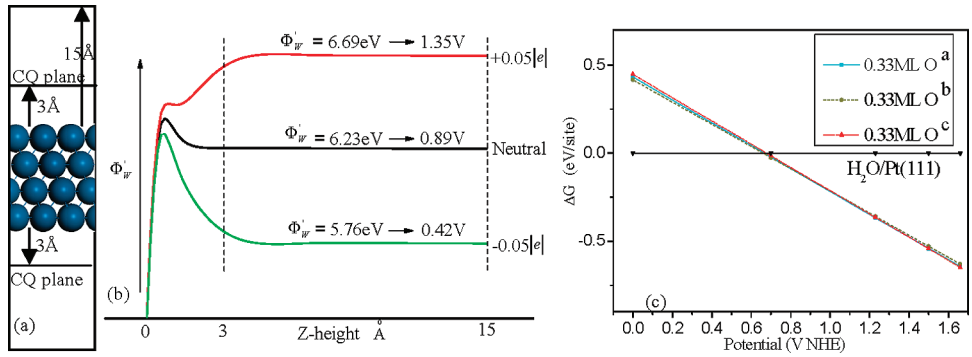

Figure 1. (a) Symmetric slab model with the counter charge (CQ) plane in vacuum. (b) Electrostatic potential averaged in *xy* plane above the Pt(111) surface (*z*-height = 0) for systems with different charges per $p(\sqrt{3} \times \sqrt{3})$ unit cell. The work function Φ_w' and the electrochemical potential can then be obtained. (c) A simple phase diagram showing the transition from H_2O/Pt(111) to 0.33 ML of O/Pt(111): [a,b] with our method, but the countercharge planes are at 3 and 2 Å above the surface, respectively, and [c] with the method proposed by Nørskov's group.[17]

is through a HOHO intermediate. Nørskov's group focused on the thermodynamic aspects of electrochemical reactions, in which the effect of electrochemical potential is simplified and taken into account by the equation $\Delta G_U = -neU$.[17,18] They suggested that an OOH intermediate could be the key species in oxygen evolution on Pt(111), which is however apparently inconsistent with the early statement from Bockris et al. that H_2O splitting is the rate-determining step in OER.[12] Other groups such as those of Neurock[19,20] and Balbuena[21,22] considered the polarization effect of electrochemical potential by adding extra charges in the periodic supercell approach, where the countercharge is homogenously distributed at the background. With a so-called double-reference method, Neurock's group showed that the electrochemical potential of the system was determined by offseting the DFT-determined work function. Interestingly, both methods from Neurock and Nørskov yielded consistent electrochemical phase diagrams for Pt and Ni in H_2O solution.[17,20,23] These pioneering theoretical works implied that the electrochemical environment, especially the dynamical solvation effect of H_2O, may be approximately represented without much loss of accuracy on the surface phase diagram.

Inspired by these works, here we develop and apply a theoretical approach based on periodic DFT calculations to model electrochemical reactions, where both effects due to the electrochemical potential and the solvation are taken into account. We focus on the surface phase diagram on the stepped Pt surface sites, which is compared with that on Pt(111), and the possibility of oxygen coupling at these metallic surface sites. From the phase diagram, we were also able to consider the thermodynamic tendency of surface oxidation in parallel to the oxygen coupling channels on the metallic sites. Our results shed some insights into the design of better anode catalysts in water electrolysis.

This paper is organized as follows. Our theoretical methods and calculation details are introduced in section 2. In section 3, our main results are presented, in which the surface phase diagrams on Pt(111) and Pt(211), the thermodynamic possibility of surface oxidation, and the oxygen coupling reaction channels on the metallic sites are reported. The solvation effect on surface phase diagram and the electric field effect on oxygen coupling barrier are also revealed in this section. A general discussion of our results is given in section 4. Finally, our conclusions are outlined in section 5.

2. Modeling and Theoretical Methods

2.1. Computational Details. All DFT calculations were performed using the SIESTA package with numerical atomic orbital basis sets and Troullier−Martins norm-conserving pseudopotentials.[24−26] The exchange-correlation functional utilized was at the generalized gradient approximation level, known as GGA-PBE.[27,28] A double-ξ plus polarization basis (DZP) set was employed. The orbital-confining cutoff was determined from an energy shift of 0.010 eV. The energy cutoff for the real space grid used to represent the density was set as 120 Ry. The Broyden method was employed for geometry relaxation until the maximal forces on each relaxed atom were less than 0.1 eV/Å. To further check the accuracy of the calculated energy of surface compositions, some key states were also examined with the plane-wave methodology as implemented in VASP package,[29−32] where the accuracies of SIESTA results are generally good and comparable to the plane-wave method (∼0.1 eV). For example, the adsorption energies of O atom with respect to $^1/_2O_2$ in the gas phase for 0.67 ML of O on the (111) surface is 0.75 eV with SIESTA and 0.66 eV with VASP. Transition states (TSs) of the catalytic reactions were searched using our constrained Broyden minimization method, as described recently.[33] It will be shown in the work that the phase diagram (mainly on the (111) surface) produced from the above DFT setups agrees with the previous calculations[17,23] and the experimental data.

In our calculations, two different-structured Pt have been chosen, namely, flat Pt(111) and stepped Pt(211) surfaces. The close-packed (111) facet is the most stable and thus dominant face for typical Pt polycrystalline, and the monatomic step represented by the (211) facet is possibly the most common structural defect, which comprises (111) terrace sites and (100) steps. These two representative surfaces were thus selected to probe the chemistry on the Pt electrode. All the surfaces were modeled with four-layer slabs, with the middle layers being fixed. For all systems with adsorbates, the adsorbates were added symmetrically on both sides of the slab and were relaxed fully. To address different coverage encountered in calculation of phase diagrams, the (111) surface was modeled by $p(\sqrt{3} \times \sqrt{3})$, $p(2 \times 2)$, and $p(4 \times 4)$ unit cells, and the stepped Pt(211) surface was modeled by $p(1 \times 2)$ and $p(1 \times 4)$ unit cells.

2.2. Theoretical Approach for Studying Electrochemistry. In our calculations, the metal slab is placed in the center of a cell and a 30 Å vacuum is introduced along the *z* direction, where we can add/subtract symmetrically adsorbed species and water layers on each side of the slab. The metal slab can then be charged by adding or subtracting a predetermined number of electrons to model the electrochemical environment. As shown in the Figure 1a, there are two symmetric surfaces (top and bottom) in slab calculations, and excess charges are evenly

distributed on both surfaces ($Q/2$). To balance the excess charge Q, the counter charge is added as two charge planes in the form of Gaussian distribution along the z direction, each with $-Q/2$. One plane is near the top surface, and the other is near the bottom surface. The Gaussian charge plane centers either at the first water layer (with water) or at a fixed z-height (typically outside the compact layer at ~3 Å) away from the outermost surface atom (without water). In the following, our approach to calculate the electrochemical potential and the total energy will be given in detail.

In order to calculate the electrochemical potential (U) of a system, the following equations can be used according to the definition of absolute electrochemical potential.[34]

$$U/V = (\Phi_w - 4.6)/\text{eV} \quad (1)$$

$$\Phi_w = \Phi_{ref} - \Phi_f \quad (2)$$

where Φ_w is the work function, which can be related to the electrochemical potential by eq 1 considering that the normal hydrogen electrode (NHE) has a measured work function of ~4.6 eV experimentally.[35] In theory, the work function Φ_w can be obtained by measuring the difference between Φ_f, the Fermi level of the system, and a predefined reference level of zero potential, i.e., the potential level in solution (far away from the surface).

However, it is practically impossible for first-principles calculations to obtain the accurate reference level because of the great difficulty in treating the long-range screening effect of water and counterionic charge in solution. In practice, we can however adopt an indirect approach, in which the experimental value for the potential of zero charge (pzc) is used to correct the calculated work function Φ_w' to yield a more reasonable Φ_w (Figure 1b)

$$\Phi_w = \Phi_w' - (\Phi_{w\,pzc}' - \Phi_{pzc}^{exp}) \quad (3)$$

where the Φ_{pzc}^{exp} is the average experimental pzc value for Pt(111), which is about 4.85 eV (0.25 V NHE).[36,37] $\Phi_{w\,pzc}'$ is the theoretical work function for neutral Pt(111) with the approximated reference level. For example, we can calculate a finite layer of H_2O-covered Pt(111) surface and use its work function as $\Phi_{w\,pzc}'$. Alternatively, we may totally omit the H_2O layer, i.e. the largest approximation, and use the calculated work function of Pt(111) as $\Phi_{w\,pzc}'$ (5.59 eV from DFT, consistent with experimental values[38,39]). For any other systems (charged or neutral), the similar condition as utilized in calculating $\Phi_{w\,pzc}'$ should be used to obtain Φ_w' and finally U (NHE). To give an example, 0.33 ML of O on Pt(111) [O/Pt(111)] with different charges were calculated and the work function Φ_w' as well as U of the system could then be obtained using eqs 1−3, as shown in Figure 1b, where the electrostatic potential averaged in the xy plane of the system is plotted against the z-height away from the surface. It shows that the reference level potential taken at the position 15 Å away from the surface is dictated by the charge of th system. Although eq 3 may not hold in all conditions, we will show later in Figure 1c that the accuracy in the calculated electrochemical potential, in fact, does not affect the calculated surface phase diagram significantly, where only the boundary points between phases are decisive. It may also be mentioned that we used the same pzc for Pt(211) as that of Pt(111), since the pzc of the defected surfaces differs only slightly.[40,41]

Next, to compare the total energy of phases with different charges, the DFT-calculated energy must be corrected. As suggested previously by Neurock's group,[19] two extra energy contributions must be removed from DFT total energy, namely, (i) the energy of the countercharge itself (E_{CQ}) and its electrostatic interaction with the charged slab ($E_{CQ-slab}$) and (ii) the energy of the excess charge in the slab ($n_Q E_F$). This is written as

$$E_{correted} = E_{DFT(n_Q,n_{CQ})} - (E_{CQ} + E_{CQ-slab}) - n_Q E_F \quad (4)$$

In our work, the countercharge is explicitly placed outside the slab in the form of a Gaussian-distributed plane charge, which is different from the previous calculations, where the countercharge is homogenously distributed in the background.[19]

For reactions involving the releasing of proton and electron, the reaction energy can be computed by referencing to the normal hydrogen electrode in a manner proposed by Nørskov's group.[18] This is governed by $G_{proton+electron} = G_{(1/2)hydrogen\ gas} - eU$ where e presents the transfer electron and U is the half-cell potential. Besides, to derive the free energy G, the DFT energy should be amended by the relevant thermodynamics terms (mainly zero point energy and the entropy contribution as tabulated in ref 18, which were also used in our work).

In Figure 1c, we give an example to show how to determine the phase diagram by using the above-mentioned methods. The horizontal line corresponds to the clean Pt(111) and H_2O, namely, the H_2O/Pt phase, which is set to zero energy. The oblique lines correspond to the 0.33 ML of O/Pt(111) phase, which were computed as follows. First, the 0.33 ML of O/Pt(111) systems with different charges (±0.15, ±0.05, and ±0.01 |e|) were calculated using DFT, in which the countercharges are placed either 2 or 3 Å above the surface. From the calculations, the corrected total energy and the electrochemical potential of each charged system can be obtained. Next, the reaction free energy values (ΔG) of H_2O/Pt → O/Pt + $2H^+$ + $2e^-$ were calculated for each charged system, and finally, the values (unit eV/site hereafter) are plotted against their electrochemical potentials. To compare with our method, the thermodynamic method proposed by Nørskov's group[17] was also used to calculate the same phases.

It is noted that the three oblique lines in Figure 1c are almost identical, and so are the phase-change potentials from the clean surface to the O-covered surface (~0.7 V). Our calculated value is slightly lower than the value (~0.8 V) reported previously,[17] which is largely due to the fact that O atoms adsorb on both sides of the slab in our approach. Figure 1 implies that the explicit polarization due to the excess charge plays a minor role in determining the surface phase diagram, since the exact position (2 or 3 Å) of the countercharge plane determines the calculated electrochemical potential from eq 3. In other words, the absolute accuracy in the calculated electrochemical potential for a system does not have a significant effect on the phase diagram. This may be understood as follows. From our calculations, the explicit polarization modifies the total energy by a much smaller extent (below 0.1 eV/V) than the term $-2eU$ does (2 eV/V). The 2eU term is required to establish the H balance between the O-covered phase and the H_2O/Pt phase (H_2O/Pt → O/Pt + $2H^+$ + $2e^-$). The slopes of the oblique lines are thus controlled by the $-2eU$ term.

3. Results

3.1. Solvation Effects on Surface Phase Diagram. At electrochemical conditions, the intimate layer (adsorbed layer) on metal electrode can be H adatoms, double-layer, hydroxyls, or oxygen adatoms, depending on the applied electrochemical potential. It is difficult to pin down the exact structure of the solid/liquid interface, even for the intimate layer, not at least

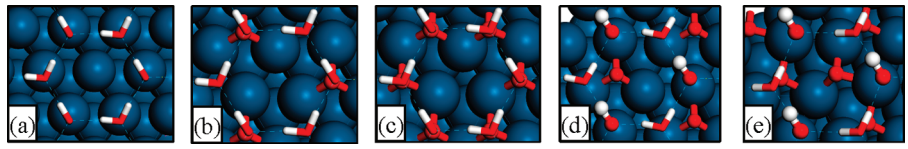

Figure 2. Optimized structures on Pt(111) in the presence of a layer of H_2O at different coverages: (a) clean surface, (b) 0.33 ML of O, (c) 0.67 ML of O, (d) 0.33 ML of O + 0.17 ML of OH, and (e) 0.67 ML of O + 0.17 ML of OH.

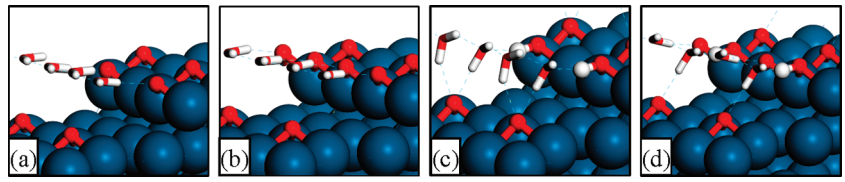

Figure 3. Optimized structures on Pt(211) in the presence of a row of H_2O near the step-edge at different coverages: (a) 0.33 ML of O, (b) 0.5 ML of O, (c) 0.17 ML of O + 0.17 ML of OH, and (d) 0.33 ML of O + 0.17 ML of OH.

because of the great mobility of H_2O at the interface. Nevertheless, at high potential ranges, where the coverage of oxidative species (O atoms, OH) on surface should be highly relevant to O_2 evolution, it is conceivable that most of the H_2O will be excluded from the intimate layer and thus the interface may be simply viewed as a "sandwich" structure, where the intimate layer lies in between the solution and the metal surface. Importantly, within this sandwich model, we can quantitatively verify the solvation effect on the adsorbed oxidative species by comparing the computed phase diagram with and without the aqueous environment. In this work, two kinds of oxidative layers on both the flat Pt(111) and stepped Pt(211) were studied to check the solvation effect on the phase diagram, namely, (i) oxygen adatoms and (ii) the mixed phase of oxygen adatoms and hydroxyls.

For Pt(111) in contact with H_2O layers, it is convenient to arrange the H_2O layer as a hexagonal bilayer ($\sqrt{3} \times \sqrt{3}$ R30° unit cell) over the surface (see Figure 2a). Such a bilayer water structure (icelike structure) was known for H_2O thin layer adsorption on close-packed metal surfaces.[5,42] In this unit cell, we are able to study the O coverage at 0.33, 0.67 ML and the corresponding O/OH mixed phases with extra 0.17 ML of OH (Figure 2b−e). In the optimized structures, as shown in Figure 2, the hydrogen bonds between the O or OH and the outer H_2O layer are available, which can help to stabilize the system. We then calculated the stability of these phases with respect to the clean surface and H_2O by using the method mentioned in section 2. On the basis of the DFT calculated energies, we found that the relative phase stability is little affected by the H_2O layer. For the O adatom phases, for example, the potential at the crossing point from the 0.33 ML of O phase to the 0.67 ML of O phase is at 1.06 V without the H_2O layer and 1.05 V in the presence of the H_2O layer. For the O and OH mixed phases, the water effect is slightly larger, but the predicted potential for the phase change is still different by no more than 0.09 V.

On the stepped Pt(211), the low-coordinated step-edge sites are present together with the (111) terrace sites. Therefore, we only need to further check the water solvation effect on the step-edge adsorbed species, which can be done by adding a row of H_2O besides the step-edge sites. Using this model, we have considered the O atom coverage of 0.33 and 0.5 ML of O, as well as the coadsorption situations containing both oxygen and hydroxyl. Hereafter for a fair comparison of coverage with that on Pt(111), the coverage of Pt(211) is defined with respect to the total exposed Pt atoms in Pt(211), i.e., three atoms per (1 × 1) cell. The representative structures are shown in Figure 3. Taking 0.33 ML of O as an example, the adsorbed oxygen in the presence of water is stabilized by about 0.07 eV per O atom, and the potential at the crossing point toward 0.5 ML of O is shifted from 0.90 to 0.96 V (0.06 V). Our calculations on Pt(211) show that although the water environment can always stabilize the oxidative species at the step-edge, the differences in the predicted potential for the phrase change are only 0.06 and 0.05 V for the pure O adatom phases and the O/OH mixed phases, respectively.

Overall, it can be seen that the water solution only has a marginal effect on the surface phase diagram concerned. This may be understood as follows. Only relative stability between phases is important to the crossing point of two phases. The solvation effect can be largely canceled out between two consecutive phases because of the similar magnitude of the water/substrate interaction. From our results, for example, in order to see appreciable potential shift (i.e., 0.1 V) at the crossing point between the 0.33 ML of O/Pt(111) and the 0.67 ML of O/Pt(111), the interaction of the H_2O layer with the additional 0.33 ML of O (=0.67−0.33) has to be about 0.4 eV per additional O atom, which is too large compared to the DFT-determined value (below 0.2 eV).

3.2. Surface Phase Diagram of Pt Surfaces from Thermodynamics. To figure out the surface phase diagram of Pt(111), we considered a series of surface phases by gradually increasing the surface coverage of O atoms, namely, 0.25, 0.50, and 0.75 ML. For a selected O coverage, we also added extra OH groups to form the O/OH mixed phases. It was noticed that the stability of the mixed phases is, however, generally close to that of the corresponding O phase at low OH coverages. For example, the phase stability of 0.75 ML of O and 0.75 ML of O + 0.0625 ML of OH is almost identical, as illustrated in the Supporting Information. Therefore, the surface phase diagram is largely dictated by the pure O atom adsorbed situations. On Pt(111) we have not explicitly modeling the H_2O layers, since its effect on the surface phase diagram is marginal, as proved above. The results are summarized in Figure 4, where the energy of the most stable phase is plotted against the applied potential (the *x*-axis). All the other less stable phases for a given potential are not shown for clarity.

From our results, the water starts to dissociate into O at 0.7 V on Pt(111). At about 1 V, we found that 0.25 and 0.5 ML of O are almost equal in stability (−0.15 eV/site). Above the potential, the 0.5 ML of oxygen overlayer is preferred thermodynamically. When the potential is higher than 1.4 V, the surface is taken over by 0.75 ML of O. These results are consistent with the previous phase diagrams calculated for Pt(111),[17,23]

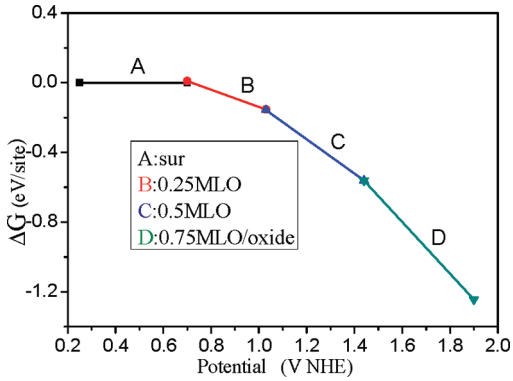

Figure 4. Surface phase diagram of Pt(111).

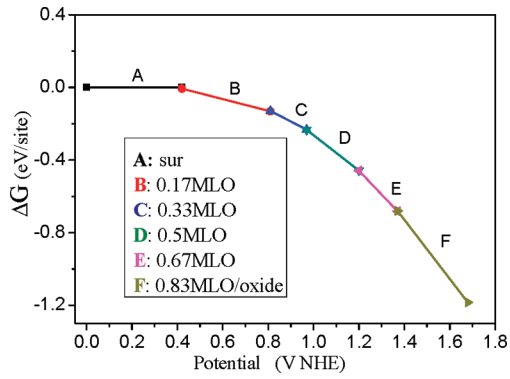

Figure 5. Surface phase diagram of Pt(211).

where the 0.25 and 0.5 ML of O phases were reported at the potential of ~0.9 and ~1.2 V, respectively.

On going to Pt(211), the surface phase becomes more complex due to the presence of stepped sites. For the same reason as Pt(111), we considered first the pure O phases on Pt(211) by gradually increasing O coverage from 0.17 to 0.83 ML. To compare with Pt(111) on a fair basis, we did not model H_2O layers on terraces but added a row of H_2O near the step-bridge of Pt(211), and the representative structures of the phases are shown in Figure 3. The surface phase diagram of Pt(211) is shown in Figure 5. The detailed data on the energetics including both the O phases and the O and OH mixed phases are tabulated in the Supporting Information. We found that on Pt(211) the step-edge bridge sites are always preferentially occupied by O. Upon further increasing O coverage, the additional O atoms will start to occupy the terrace sites, and only above 0.83 ML of O will the lower step sites be occupied.

It is of interest to compare the phase diagram on Pt(211) with that on Pt(111). At relatively low potentials, say below 0.7 V, when Pt(111) is still dominated by water bilayers, Pt(211) is already covered by O atoms. The 0.17 ML of O appears on Pt(211) as early as about 0.4 V. This agrees with the fact that Pt defect sites covered by oxygen species has been monitored under low potentials (~0.4 V) in electrochemical experiment.[43] At potentials near 0.8 V, Pt(211) is dominated by 0.33 ML of O, while at the same potentials the O coverage on Pt(111) is only 0.25 ML. Obviously, this is because the stepped sites tend to bond species more strongly and thus enable H_2O splitting into the oxidative species at relatively low potential. The 0.5 ML of oxygen overlayer on Pt(211) is preferred thermodynamically above 0.97 V. In succession, Pt(211) will be occupied by the 0.67 ML of O from 1.2 to 1.37 V. When the potential is above 1.37 V, the surface composition is dominated by the 0.83 ML of O.

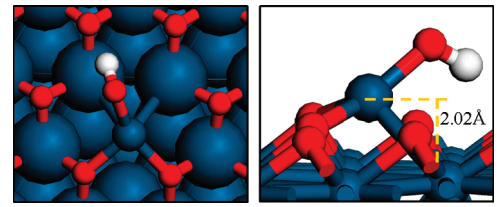

Figure 6. Top and side view structures of the 0.75 ML of O + 0.0625 ML of OH covered Pt(111).

3.3. Surface Oxidation at High Potentials from Thermodynamics. It is naturally expected that at high potentials the surface oxidation may evolve. From our DFT structural optimization, we noticed that Pt surface atoms start to move out from the surface plane at high O surface coverages. On Pt(111), for example, at about 1.4 V, a Pt−Pt bond increases evidently from the original 2.89 to 4.83 Å at the 0.75 ML of O + 0.0625 ML of OH coverage, as illustrated in Figure 6. To verify whether surface oxides may form at these conditions, we calculated the stability of the subsurface O phases, where an oxygen atom per cell sits at the subsurface, to compare with the stability of the surface O phases mentioned above. Our results showed that the O subsurface phase is less stable (by 0.72 eV) than the surface O phase at the stage of 0.5 ML of O + 0.0625 ML of OH coverage (about 1 V) of Pt(111). However, it is already stable (by 0.31 eV) at 0.75 ML of O + 0.0625 ML of OH coverage. This implies that the surface oxidation on (111) terraces is thermodynamically favored above 1.4 V. Experimentally, Pt surface oxidation has been clearly observed, for example, by Jerkiewicz et al. and Tian et al.,[44,45] which showed that the oxidation is, however, kinetically slow at 1.2 V. It should be emphasized that our study was performed with the periodic slab model and the coverage investigated is largely limited by the unit cell chosen. Since our calculation showed that at 1.4 V [0.75 ML of O/Pt(111)], the subsurface oxygen is already more stable than the surface oxygen, it is expected that the surface oxidation can already occur at a potential in between 1 V (0.5 ML of O) and 1.4 V (0.75 ML of O), as dictated by thermodynamics. On the other hand, at low O coverages (e.g., 0.25 ML of O), the subsurface O phases were calculated previously and found to be unstable, where the surface O requires a high barrier to diffuse into the subsurface.[46−48]

3.4. Reaction Channels of Oxygen Coupling Reaction. The phase−potential diagrams determined above enable us to evaluate the reaction kinetics for oxygen evolution at a given electrochemical potential. Since the surface coverage is closely related to the electrochemical potential, a linkage can be established between reactivity and electrochemical potential by studying the reaction channels at different surface coverages. There are three possible oxygen coupling pathways, namely, O + O → O_2, O + OH → OOH, and OH + OH → HOOH. For these three possibilities, we have searched for all the likely reaction pathways at different surface coverages on both Pt(111) and (211) surfaces. Our results for Pt(111) are summarized in Table 1 and those for Pt(211) are in Table 2.

Among the three possible coupling pathways on Pt(111), the coupling of adsorbed O atoms is the simplest and has been well-investigated previously in the context of UHV conditions. Over the late transition metals, such as Ru, Rh, and Pt, the O + O coupling reaction is found to be highly activated at low O coverages.[13] Consistently, our calculations also show that the reaction barrier for the coupling between two adsorbed O is higher up to about 2 eV at low O coverages. With the increase of surface O coverage, the barrier of the O + O reaction is

TABLE 1: Quasidifferential Oxygen Adsorption Energy [E_{ad}(O)] and Reaction Barrier (E_a) for Oxygen Coupling Reactions on Pt(111)

reaction path	surface intermediates	E_{ad}(O) (eV)	E_a (eV)
O + O reaction	0.5 ML of O	0.44	1.89
	0.67 ML of O	0.36	1.69
	0.75 ML of O	−0.40	1.15
	1 ML of O	−1.43	1.00
O + OH reaction	0.25 ML of O + 0.25 ML of OH	1.04	1.57
	0.5 ML of O + 0.25MLOH	−0.21	1.21
	0.75 ML of O + 0.0625 ML of OH	−0.76	1.60

TABLE 2: Quasidifferential Oxygen Adsorption Energy [E_{ad}(O)] and Reaction Barrier (E_a) for Oxygen Coupling Reactions on Pt(211)

reaction path	surface coverage	E_{ad}(O) (eV)	E_a (eV)
O + O reaction	0.33 ML of O	0.91	1.79
	0.5 ML of O	0.26	1.32
	0.67 ML of O	0.11	1.23
	0.83 ML of O	−0.51	0.95
	1 ML of O	−0.89	0.83
O + OH reaction	0.17 ML of O + 0.17 ML of OH	1.10	1.81
	0.33 ML of O + 0.17 ML of OH	0.46	1.33
	0.5 ML of O + 0.17 ML of OH	0.01	1.17
	0.67 ML of O + 0.17 ML of OH	−0.25	1.19
	0.83 ML of O + 0.17 ML of OH	−0.83	0.50

reduced, but it is still around 1 eV even at the saturated 1 ML of O coverage. The reduction of the barrier can be attributed to thermodynamics. As listed in Table 1, we have calculated the quasidifferential oxygen adsorption [E_{ad}(O)] with respect to the gas phase O_2 through the equation $E_{ad}(O) = E_{((n-1)O+mOH)/Pt} + {}^1/_2E_{O_2(gas)} - E_{(nO+mOH)/Pt}$, where E_X is the DFT total energy of X and n and m are the numbers of O atom and OH in the unit cell, respectively. A positive E_{ad}(O) means that the adsorbed O is more stable than it in the gas phase as O_2. Table 1 reveals that the adsorbed oxygen atom becomes less stable with the increase of O coverage, which drives the oxygen coupling thermodynamically.

For the O + OH reaction channel on Pt(111), the reaction barriers are not so much different from their O + O counterparts. However, it is noticed that at the highest coverage conditions, 0.75 ML of O + 0.0625 ML of OH, the barrier identified for the O + OH reaction increases instead. This abnormal barrier increase is caused by the significant structural relaxation of surface Pt atom at this highest coverage, where the surface Pt atom beneath the OH moves out significantly from the surface plane by more than 2.0 Å, as shown in Figure 6. From this initial structure, it is difficult for the atop OH to react with the nearby O that sits at the surface plane.

For the OH + OH reaction channel, we found that this channel is kinetically inhibited. Even at the high O coverage conditions (0.5 ML of O + 0.5 ML of OH), the reaction barrier is still very high (1.59 eV), which indicates that this reaction cannot occur at ambient conditions.

In Figure 7, we highlight the identified TSs for the O + O reaction at 0.75 ML and the O + OH reaction at 0.75 ML of O + 0.0625 ML of OH coverage conditions. For the O + O reaction at 0.75 ML, the TS is achieved when one O is sitting at the bridge site and another O is at the atop site. Because of

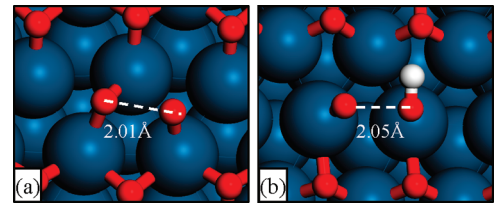

Figure 7. Located TS structures on Pt(111) for (a) O + O reaction at 0.75 ML of O coverage and (b) O + OH reaction at 0.75 ML of O + 0.0625 ML of OH coverage.

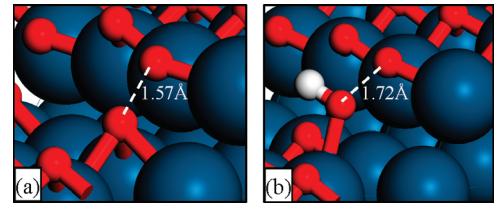

Figure 8. Located TS structures on Pt(211) for (a) O + O reaction at 0.83 ML of O coverage and (b) O + OH reaction at 0.83 ML of O + 0.17 ML of OH coverage.

the local high coverage of O atoms, the TS O−O complex has a quite short distance (2.96 Å) to its neighboring O atoms. For the O + OH reaction, the TS is achieved when both the OH and the O stand on the atop sites of adjacent Pt atoms. In general, at least one oxygen atom has to shift from its original fcc hollow site to the atop site in order to couple with another O or OH species on Pt(111). Since the potential energy surface of O atom is rather corrugated (the atop O is much less stable than the hollow-site O), it is not surprising that the determined barrier on Pt(111) is always more than 1 eV.

On Pt(211), we focused on the reaction channels of O + O and O + OH. The quasidifferential adsorption energy of O [E_{ad}(O)] as defined above was also calculated and is summarized in Table 2. From Table 2, we can see that the reaction barrier also decreases with the increase of surface coverage, which is accompanied by the decrease of E_{ad}(O). For example, the barrier of the O + O reaction drops from 1.79 eV at the 0.33 ML coverage to 0.83 eV at the 1 ML coverage. More importantly, the O + OH reaction occurring at the stepped sites can have a lower barrier than the O + O reaction on Pt(211). The lowest barrier of the O + OH reaction channel is only 0.50 eV at the 0.83 ML of O + 0.17 ML of OH coverage. We then further checked this reaction channel at a lower OH coverage (0.83 ML of O + 0.083 ML of OH) by doubling the unit cell, which corresponds to the electrochemical potential of 1.37 V. At this coverage, the determined barrier is 0.64 eV, which is still low enough for the O + OH to occur at room temperature.

The TS structures for the O + O reaction and the O + OH reaction of the lowest barriers on Pt(211) are illustrated in Figure 8. The other TSs are shown in the Supporting Information. At the TS for the O + O reaction at 0.83 ML of O/Pt(211), one O is at the step-bridge site and the other O is at the lower terrace hollow site near the step. It should be mentioned that such diatomic TSs at transition metal steps are well-known for CO, NO, and N_2 dissociation reactions.[49−51] Because the TS involves a total of five metal atoms in bonding and there is no so-called bonding competition effect at the TS, the TS is more stable than its counterpart on terraces, and thus, the reaction barrier can be reduced. For the O + OH reaction at high coverage conditions, e.g. 0.83 ML of O + 0.17 ML of OH, the TS structure is reached in a similar manner to the O + O reaction, where the O is at the step-bridge site and the OH is at the lower-step atop site.

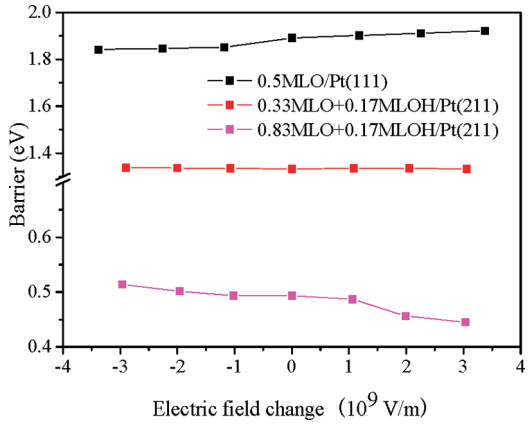

Figure 9. Oxygen coupling barrier on charged surfaces as indicated by the change of electric field. The zero on the *x*-axis corresponds to the neutral situations as tabulated in Tables 1 and 2.

A key feature of these TSs is that the O or OH remains at the initial adsorption position at the TSs, which is different from the TSs on (111) terrace sites.

3.5. Effect of Local Electric Fields on the Barrier of Oxygen Coupling Reactions. Having considered all the possible reaction channels at different surface coverages, we are at the position to further check whether the variation of the electric field (the charged surface) can influence directly the barrier of oxygen coupling reactions. In our method, the electric field can be tuned facilely by adding or subtracting the charge of the system. From the neutral system to the charged system, the electric fields on the surface are strongly changed and thus the barrier may be varied. The barrier vs the change of the electric field is thus examined in Figure 9. The zero on the *x*-axis corresponds to the neutral situation where the barriers are tabulated in Tables 1 and 2. In our calculations, we have researched the TS at each electric field condition, which show that there is only a small geometrical change for the reaction complex (O−O and O−OH) at the TS (the structural data at the TS for the O + OH reaction is shown in the Supporting Information). Our results show that the effect of the electric field induced by the excess surface charge plays only a minor role on influencing the reaction barrier, where the magnitude is below 0.1 eV per change of 10^9 V m^{-1}. This is true at all coverages and on both surfaces. Our results are consistent with the recent theoretical studies showing that the barrier of the oxygen reduction reaction is only little affected by electric fields.[23] Considering that the electric field at the anode is typically in the range of 10^8-10^{10} V m^{-1}, we may conclude that the electrochemical potential shift does not change significantly the reaction barrier in a direct manner. Instead, the potential variation can adjust the surface coverage of oxidative species on the surface, which can effectively reduce/increase the barrier of oxygen coupling reactions.

4. General Discussion

The ultimate aim of theoretical calculations on electrochemical reaction is to establish a predictive basis for the design and the optimization of catalysts. This study shows that the oxygen coupling reactions on metallic Pt sites are generally difficult, which may start to occur as late as 1.4 V, when the surface can in fact undergo oxidation with the surface O penetration into the sublayers. While the Pt metal sites under high potential ends are already not accessible by experiment, our calculations on different oxygen coupling reactions from low to high potentials on different-structured Pt sites demonstrate that the oxygen coupling reaction is strongly surface structure sensitive and thus provide new insights into the OER reaction on Pt anode. From our results, we may outline two factors that affect the electrocatalytic activity: (i) the adsorption energy of oxidative species and (ii) the surface local structure. We showed that Pt surface has a strong oxygen-bonding ability at low coverages. The overpotential is needed for increasing the surface coverage and reducing the adsorption energy of oxidative species. The adsorption energy of oxidative species is thus the essential thermodynamic factor. More importantly, we showed that an optimum surface structure is kinetically essential for the oxygen coupling reaction. Provided with the similar O adsorption energy, only stepped surface sites can help the coupling between O and OH. This is largely due to the fact that the oxygen atom on the (111) surface must shift from its original fcc hollow site to the atop site in order to couple with another O or OH species, which induces a significant energy cost.

Experimentally, the determined apparent activation energy is 0.67 eV at 1.5 V on a Pt wire anode, while the measured current density ($-\log i$) is extremely low ($\sim$7).[12] From kinetic equations, we can deduce that the population of active sites for oxygen evolution on the Pt anode is around 0.01% of the total sites (assuming that the preexponential factor for the rate-determining step is 10^{13}), which is obviously too low for an active catalyst. The lack of active sites on the oxide-covered Pt anode suggested that the key elementary step in OER reaction may only take place at minority surface sites. This is apparently consistent with our results that the oxygen coupling reaction is surface structure sensitive and only occurs at the sites where the O atom has a low coordination.

A good anode catalyst for oxygen evolution must, in general, have a low overpotential η (below $\sim$0.3 V) and a large apparent current density (e.g., below 1 on the scale of $-\log i$).[52] The Pt anode is obviously not qualified for the lack of active sites. On the other hand, the performance of other late transition metal oxides (e.g., RuO_2, IrO_2) is far better, as known from experiment.[10] This may not be totally surprising, since the O and OH adsorption on these metal oxides is usually at the atop sites of the exposed coordinately unsaturated metal ions[53] seen from the rutile phase of these oxides. The oxygen coupling reaction on them should therefore be similar to those that happened on Pt(211), where the O and OH stay at their initial adsorption position to react. Another advantage of these oxide materials may be the high density of the exposed coordinately unsaturated metal ions, which are widely available even on the most stable surface facets such as (110) of RuO_2.[53] It is therefore interesting in the future work to explore the possible structure of Pt surface oxides and to understand from the atomic level why Pt surface oxides are not good catalysts for OER reaction considering that the apparent barrier determined from experiment is not high.[12]

5. Conclusions

This work represents a theoretical attempt to obtain an overview of the surface phase diagram of Pt, including both the flat and the stepped surface, and to understand the oxygen coupling channels on the different-structured Pt under electrochemical conditions. A new approach based on periodic density functional theory calculations was implemented to mimic the electrochemical environment. In the approach, the surface is explicitly polarized by add/subtracting charges, and the countercharges are placed as Gaussian-distributed plane charges in a vacuum. With this method, the surface phase diagrams for both the closed-packed Pt(111) and stepped (211) are deter-

mined. We show that stepped surface sites can better accumulate oxidative species (O and OH) and thus reach to a higher local O coverage than terrace sites do at the same potential condition. The effect of water environment on surface phase diagram is quantitatively evaluated and found to be small.

All oxygen coupling reaction channels on Pt surfaces at different potentials are then examined. We found that the electric field induced by the excess surface charge does not affect significantly the barrier of the oxygen coupling reaction. Instead, the local surface coverage and the surface structure are much more important to the barrier. At low overpotentials, the oxygen coupling reaction on Pt metal is kinetically difficult with high barriers. An O + OH → OOH reaction can eventually occur at a high local coverage of the stepped sites (at ~1.4 V) with the calculated barrier lower than 0.7 eV. By contrast, no facile O coupling channels exist on Pt(111), as the barriers are no less than 1 eV. In parallel to oxygen coupling on these metallic sites, we also show from thermodynamics that the surface oxidation of Pt can already occur below 1.4 V with the surface O penetration into sublayers. This indicates that oxygen evolution on Pt anode occurs on Pt surface oxides, as dictated by thermodynamics. The strong structure sensitivity of the oxygen coupling reaction on metallic sites shown here may also be extended to understand why Pt is not a good anode material for oxygen evolution.

Acknowledgment. This work is supported by NSF of China (20825311, 20773026, 20721063, J0730419) and Science & Technology Commission of Shanghai Municipality (08DZ2270500). Shanghai Supercomputing Center is thanked for computing time.

Supporting Information Available: Potential-dependent reaction free energies at 0.75 ML of O and 0.75 ML of O + 0.0625 ML of OH on Pt(111), located TS structures on Pt(211) at different coverages, surface phases (both O and O/OH mixed phases) and their stability as measured by ΔG on Pt (211) at different potentials, the TS structure of O + OH reaction at the 0.83 ML of O +0.17 ML of OH on Pt(211) under the change of electric field, and reaction energetics of O + OH → OOH and OOH → O_2 + H^+ + e^- on Pt(211). This material is available free of charge via the Internet at http://pubs.acs.org.

References and Notes

(1) Hammer, B.; Norskov, J. K. *Adv. Catal.* **2000**, *45*, 71.
(2) Liu, Z. P.; Hu, P. *Top. Catal.* **2004**, *28*, 71.
(3) Studt, F.; Abild-Pedersen, F.; Bligaard, T.; Sorensen, R. Z.; Christensen, C. H.; Norskov, J. K. *Science* **2008**, *320*, 1320.
(4) Somorjai, G. A. *Introduction to Surface Chemistry and Catalysis*; John Wiley & Sons Inc.: New York, 1994.
(5) Ogasawara, H.; Brena, B.; Nordlund, D.; Nyberg, M.; Pelmenschikov, A.; Pettersson, L. G. M.; Nilsson, A. *Phys. Rev. Lett.* **2002**, *89*, 276102.
(6) Pajkossy, T.; Kolb, D. M. *Electrochem. Commun.* **2007**, *9*, 1171.
(7) Norskov, J. K.; Rossmeisl, J.; Logadottir, A.; Lindqvist, L.; Kitchin, J. R.; Bligaard, T.; Jonsson, H. *J. Phys. Chem. B* **2004**, *108*, 17886.
(8) Beni, G.; Schiavone, L. M.; Shay, J. L.; Dautremontsmith, W. C.; Schneider, B. S. *Nature* **1979**, *282*, 281.
(9) Bockris, J. O. M. *Int. J. Hydrogen Energy* **1999**, *24*, 1.
(10) Trasatti, S. *Electrochim. Acta* **1984**, *29*, 1503.
(11) Marshall, A. T.; Sunde, S.; Tsypkin, A.; Tunold, R. *Int. J. Hydrogen Energy* **2007**, *32*, 2320.
(12) Damjanov, A.; Dey, A.; Bockris, J. O. M. *Electrochim. Acta* **1966**, *11*, 791.
(13) Norskov, J. K.; Bligaard, T.; Logadottir, A.; Bahn, S.; Hansen, L. B.; Bollinger, M.; Bengaard, H.; Hammer, B.; Sljivancanin, Z.; Mavrikakis, M.; Xu, Y.; Dahl, S.; Jacobsen, C. J. H. *J. Catal.* **2002**, *209*, 275.
(14) Bard, A. J.; Faulkner, L. R. *Electrochemical Methods: Fundamentals and Applications*, 2nd ed.; John Wiley & Sons Inc.: New York, 2001.
(15) Bianchi, I.; Guerrini, E.; Trasatti, S. *Chem. Phys.* **2005**, *319*, 192.
(16) Anderson, A. B.; Albu, T. V. *Electrochem. Commun.* **1999**, *1*, 203.
(17) Rossmeisl, J.; Norskov, J. K.; Taylor, C. D.; Janik, M. J.; Neurock, M. *J. Phys. Chem. B* **2006**, *110*, 21833.
(18) Rossmeisl, J.; Logadottir, A.; Norskov, J. K. *Chem. Phys.* **2005**, *319*, 178.
(19) Filhol, J. S.; Neurock, M. *Angew. Chem., Int. Ed.* **2006**, *45*, 402.
(20) Taylor, C.; Kelly, R. G.; Neurock, M. *J. Electrochem. Soc.* **2006**, *153*, E207.
(21) Wang, Y. X.; Balbuena, P. B. *J. Phys. Chem. B* **2004**, *108*, 4376.
(22) Wang, Y. X.; Balbuena, P. B. *J. Phys. Chem. B* **2005**, *109*, 14896.
(23) Hansen, H. A.; Rossmeisl, J.; Norskov, J. K. *Phys. Chem. Chem. Phys.* **2008**, *10*, 3722.
(24) Soler, J. M.; Artacho, E.; Gale, J. D.; Garcia, A.; Junquera, J.; Ordejon, P.; Sanchez-Portal, D. *J. Phys.: Condens. Matter* **2002**, *14*, 2745.
(25) Junquera, J.; Paz, O.; Sanchez-Portal, D.; Artacho, E. *Phys. Rev. B* **2001**, *64*, 235111.
(26) Troullier, N.; Martins, J. L. *Phys. Rev. B* **1991**, *43*, 1993.
(27) Perdew, J. P.; Wang, Y. *Phys. Rev. B* **1992**, *45*, 13244.
(28) Perdew, J. P.; Chevary, J. A.; Vosko, S. H.; Jackson, K. A.; Pederson, M. R.; Singh, D. J.; Fiolhais, C. *Phys. Rev. B* **1992**, *46*, 6671.
(29) Kresse, G.; Hafner, J. *Phys. Rev. B* **1993**, *47*, 558.
(30) Kresse, G.; Hafner, J. *J. Phys.: Condens. Matter* **1994**, *6*, 8245.
(31) Kresse, G.; Hafner, J. *Phys. Rev. B* **1994**, *49*, 14251.
(32) Vanderbilt, D. *Phys. Rev. B* **1990**, *41*, 7892.
(33) Wang, H. F.; Liu, Z. P. *J. Am. Chem. Soc.* **2008**, *130*, 10996.
(34) Tsiplakides, D.; Archonta, D.; Vayenas, C. G. *Top. Catal.* **2007**, *44*, 469.
(35) Reiss, H.; Heller, A. *J. Phys. Chem.* **1985**, *89*, 4207.
(36) Cuesta, A. *Surf. Sci.* **2004**, *572*, 11.
(37) Iwasita, T.; Xia, X. H. *J. Electroanal. Chem.* **1996**, *411*, 95.
(38) Ranke, W. *Surf. Sci.* **1989**, *209*, 57.
(39) Kiskinova, M.; Pirug, G.; Bonzel, H. P. *Surf. Sci.* **1985**, *150*, 319.
(40) Gomez, R.; Climent, V.; Feliu, J. M.; Weaver, M. J. *J. Phys. Chem. B* **2000**, *104*, 597.
(41) Climent, V.; Attard, G. A.; Feliu, J. M. *J. Electroanal. Chem.* **2002**, *532*, 67.
(42) Vassilev, P.; van Santen, R. A.; Koper, M. T. M. *J. Chem. Phys.* **2005**, 122.
(43) Markovic, N. M.; Ross, P. N. *Surf. Sci. Rep.* **2002**, *45*, 121.
(44) Jerkiewicz, G.; Vatankhah, G.; Lessard, J.; Soriaga, M. P.; Park, Y. S. *Electrochim. Acta* **2004**, *49*, 1451.
(45) Tian, N.; Zhou, Z. Y.; Sun, S. G.; Ding, Y.; Wang, Z. L. *Science* **2007**, *316*, 732.
(46) Gu, Z. H.; Balbuena, P. B. *J. Phys. Chem. C* **2007**, *111*, 9877.
(47) Gu, Z. H.; Balbuena, P. B. *J. Phys. Chem. C* **2007**, *111*, 17388.
(48) Gu, Z. H.; Balbuena, P. B. *J. Phys. Chem. C* **2008**, *112*, 5057.
(49) Liu, Z. P.; Jenkins, S. J.; King, D. A. *J. Am. Chem. Soc.* **2004**, *126*, 10746.
(50) Andersson, M. P.; Abild-Pedersen, E.; Remediakis, I. N.; Bligaard, T.; Jones, G.; Engbwk, J.; Lytken, O.; Horch, S.; Nielsen, J. H.; Sehested, J.; Rostrup-Nielsen, J. R.; Norskov, J. K.; Chorkendorff, I. *J. Catal.* **2008**, *255*, 6.
(51) Liu, Z. P.; Hu, P. *J. Am. Chem. Soc.* **2003**, *125*, 1958.
(52) Singh, R. N.; Mishra, D.; Anindita; Sinha, A. S. K.; Singh, A. *Electrochem. Commun.* **2007**, *9*, 1369.
(53) Rossmeisl, J.; Qu, Z. W.; Zhu, H.; Kroes, G. J.; Norskov, J. K. *J. Electroanal. Chem.* **2007**, *607*, 83.

JP901091A